

University of Texas Rio Grande Valley

ScholarWorks @ UTRGV

Civil Engineering Faculty Publications and
Presentations

College of Engineering and Computer Science

2023

Finite element analysis of compaction load to investigate the stress-deformation behavior of soil geosynthetic composite mass: A case study

Truc Phan

Meen-Wah Gui

Thang Pham

Follow this and additional works at: https://scholarworks.utrgv.edu/ce_fac



Part of the [Civil Engineering Commons](#)

PAPER • OPEN ACCESS

Finite element analysis of compaction load to investigate the stress-deformation behavior of soil geosynthetic composite mass: A case study

To cite this article: Truc Phan *et al* 2023 *IOP Conf. Ser.: Mater. Sci. Eng.* **1289** 012105

View the [article online](#) for updates and enhancements.

You may also like

- [Comparative Study of Light Manipulation in Three-Level Systems Via Spontaneously Generated Coherence and Relative Phase of Laser Fields](#)
Nguyen Huy Bang, Le Nguyen Mai Anh, Nguyen Tien Dung et al.
- [Probe gain via four-wave mixing based on spontaneously generated coherence](#)
Hong Yang, , Ting-gui Zhang et al.
- [Constraining the H i-Halo Mass Relation from Galaxy Clustering](#)
Hong Guo, Cheng Li, Zheng Zheng et al.



245th ECS Meeting • May 26-30, 2024 • San Francisco, CA

Don't miss your chance to present!

Connect with the leading electrochemical and solid-state science network!

Deadline Extended: December 15, 2023

Submit now!



Finite element analysis of compaction load to investigate the stress-deformation behavior of soil geosynthetic composite mass: A case study

Truc Phan^{1,*}, Meen-Wah Gui², Thang Pham³

¹ Department of Bridge and Road, Mien Trung University of Civil Engineering, Phu Yen 620000, Vietnam

² Department of Civil Engineering, National Taipei University of Technology, Taipei 10608, Taiwan

³ Department of Civil Engineering, University of Texas Rio Grande Valley, TX 78539, United States

* Corresponding author's e-mail: phantranhanhtruc@muce.edu.vn

Abstract. When building Soil Geosynthetic Composite (SGC) walls, fill compaction is normally carried out by operating a compactor in a general direction parallel to the wall face. In other words, a moving point or area load is often used to apply a compaction load on a newly installed soil lift. Pham (2009) and Wu and Pham (2010) demonstrated that the compaction-induced stress (CIS) caused by multiple passes of a compactor moving toward or away from a section can be calculated by taking into account the compaction load applied directly above the section under consideration using a simplified stress path proposed by Duncan and Seed (1986). Additionally, by simulating the compaction, the CIS due to fill compaction may be correctly assessed. The CIS resulting from fill compaction can also be accurately assessed by simulating the compaction load, such as by applying a distribution load on top of each backfill layer or a distribution load at the top and bottom of each soil layer, or by applying various widths of strip load to the top of each backfill layer. The objective of this study was to validate the numerical simulation of the compaction load to stress deformation behavior of SGC mass under operating stress conditions. In order to conduct the numerical analysis, data from both a full-scale instrumented SGC mass based on large-scale soil geosynthetic composite (SGC) experiments and a 6 m-high SGC (Pham, 2009) were employed. This study will examine a few SGC behavior parameters, including reinforcement strains, lateral displacements, and reinforcement strains. The objective of the FE modeling is to demonstrate the effect, emphasize the significance of the compaction conditions to the stress-deformation behavior of SGC mass, and validate the findings from the field-scale experiments and proposed model by Pham (2009) and Wu and Pham (2010).

1. Introduction

In order to achieve and maintain stability, metallic strips were added to the compacted fill along with a wall face in the 1960s. Later, polymeric geosynthetics were utilized as reinforcement in place of metallic strips. These reinforced soil walls are typically designed using techniques from the FHWA method [6], the NCMA method (National Concrete Masonry Association [24], and AASHTO specifications American Association of State Highway and Transportation Officials [4].



MSE walls reinforced with geosynthetics can be addressed as Geosynthetic Mechanically Stabilized Earth (GMSE). For GMSE walls, reinforcement spacing typically ranges between 0.3 and 0.9 m. The fundamental design principle of a tieback system is what causes the comparatively wide spacing. The total resisting force in a tieback system matters more than the tieback spacing, which is of very little importance. But in recent years, awareness of the significant advantages of using sheet reinforcement on small spacings has grown.

In recent years, awareness of the major advantages of installing sheet reinforcement with close spacing has grown. Close reinforcement spacing has considerable advantages that were initially seen during construction and afterward confirmed by several field-scale investigations [1,2,15,25-26,34]. These tests have demonstrated that, in terms of a reinforced soil system's capability, reinforcement spacing is important considerably more than reinforcement strength. A soil geosynthetic composite (SGC), which correctly describes the behavior of reinforced soil with closely spaced geosynthetic reinforcement, has also been constructed.

Numerous authors have studied "Compaction Induced Stress" (CIS) in soil masses, including [3,9,11,26,32,39-40]. The concept of average stress, a theory of soil-geosynthetic composite behavior proposed by [19], and a simplified stress path that was developed by [39] for an unreinforced soil mass. They demonstrated that the compaction-induced stress (CIS) at any given section due to multiple passes of a compactor moving toward or away from the section under study is caused by the concept of average stress.

In order to analyze the behavior of GRS walls, numerical methods are now frequently used [16-17,20-23,30,42-43]. The numerical methods have many advantages over laboratory experiments and field measurements, including obtaining more thorough results, examining the effects of various loading conditions, and researching the effects of various variables and parameters, which are challenging or expensive to achieve in laboratory and field tests. To assess the composite behavior of the GRS walls under static loading, two-dimensional (2D) numerical modeling studies have been carried out [26-28,36-38,44].

As with applying a uniform load to the top of each backfill layer when modeling the wall from the bottom up [5,16-18,26,28,36-37,39-40,43], another method of modeling the compaction load is to apply a distribution load to Compaction of each soil lift was simulated in FE analysis and SGC tests by placing a uniform equivalent compaction pressure of 44 kPa on top of the freshly placed soil and removed the applied compaction pressure before placing the next soil lift and noted that the compaction energy used in the GSGC tests was very low. As a result, the magnitude of CIS was very small, and the effect of CIS on the global stress-strain relationship was not significant.

The objective of the present study is to verify numerical modeling of CIS that is related to some issues of the stress-deformation behavior of soil geosynthetic composite mass, such as compaction-induced stresses, stress, and strain in reinforcements and compaction induced stresses of a soil geosynthetic composite using data from a full-scale GRS wall under working stress conditions [26]. Note that the results from this full-scale GRS wall have already been utilised for validation in several other numerical model studies [26,36-37,39,41]. However, in the five SGC tests had the same for compaction conditions for each soil that related to the vibrating plate compactor used on the testes with a compaction stress value of 44 kPa were used in the numerical analyses.[37] identified that the equivalent compaction load for GRS walls is likely to be affected by factors such as modeling the compaction load, soil type, soil placement condition, compactor type, compaction lift thickness, boundary conditions, and the soil model employed in the analysis. For example, for modeling the compaction load issue, compaction can be accurately evaluated by modeling the compaction load as a point or limited-area load (footprint of the compactor) at a critical section, not by a strip load or a uniform load applied over the entire surface area of a newly placed soil lift.

These uncertainties led to the variation in the equivalent compaction load and the application method. This is a major difficulty with the equivalent compaction load approach. So that, investigating the effect of some parameters of compaction load, such as typical compaction process, the equivalent load, and modeling load to composite behavior of SGC mass to achieve compaction efficiency is needed.

where OCR and ϕ are the over-consolidation and internal friction angle, respectively. [7] has developed a compaction theory which sets limits of CIS value for unreinforced soil as:

$$0.45\sqrt{Q\gamma} \leq \text{CIS} \leq 0.90\sqrt{Q\gamma} \quad (3)$$

where γ is the as-compacted unit weight of the fill material, and Q is the maximum force per unit length of the compactor (imposed by joint action of gravity and cyclic acceleration). [3] stated that using Bolton's upper limit and lower limit of CIS value and may be adopted for preliminary design and analysis of GRS structures.

From the Table 1 a, b gives example calculations of CIS for light soil compacting types of equipment (vibratory plate compactor) and heavy soil compacting types of equipment (roller compactors) from authors and some compactors from manufactures.

Table 1. Data for soil compacting equipment.

(a) Data for vibratory plate soil compactor

Manufacturer	Model	Plate width (m)	Total force (kN/m)	$0.45\sqrt{Q\gamma}$	$0.90\sqrt{Q\gamma}$	Referred to
Bomag	BP 10/36	0.361	27.600	10.260	20.530	[10]
Wacker	VPG 160B	0.533	21.100	8.970	17.950	-
Wacker	VPG 160R	0.533	22.360	9.240	18.480	-
Wacker	VPG 160 A	0.533	22.440	9.260	18.510	-
Ingersoll-Rand	BX-6	0.406	30.490	10.790	21.580	-
Bomag	BP 13/29	0.290	43.820	12.930	25.870	-
Wacker	BPS 1330R	0.305	43.430	12.880	25.750	-
Wacker	BPS 1330	0.305	43.460	12.880	25.760	-
Case	1300	0.495	37.630	11.980	23.970	-
Wacker	BPU 2440A	0.394	64.200	15.650	31.310	-
Wacker	BPS 2550B	0.495	53.320	14.270	28.530	-
Bomag	BP30	0.381	79.950	17.470	34.940	-
Wacker	BPU 2950R	0.495	61.820	15.360	30.720	-
Bomag	BP34	0.650	58.610	14.960	29.910	-
Wacker	BPU 3345R	0.673	54.200	14.380	28.770	-
Bomag	BP 50	0.599	83.860	17.890	35.780	-
Wacker	DPU 5055	0.711	76.510	17.090	34.180	-
Wacker	DPU 6760	0.800	91.060	18.640	37.290	-
Wacker	VPG 155 -A	0.460	34.120	11.410	22.830	[5]
Wacker	ES-45-Y	0.250	48.000	13.540	27.070	-
Dynapac	DFP12D	0.500	52.460	14.150	28.300	[8,12]
Dynapac	DRP15X	0.500	52.800	14.200	28.390	-
Dynapac	DFP11	0.500	52.160	14.110	28.220	-
Dynapac	DRP25D	0.600	71.000	16.460	32.930	-
Dynapac	DRP70D	0.500	214.100	28.590	57.180	-
Bomag	BP 20/50	0.500	41.900	12.650	25.290	-
Bomag	BVP 18/45	0.360	52.500	14.160	28.310	-

Bomag	BPR 35/60 D	0.600	63.700	15.590	31.190	-
Bomag	BPR 35/42 D	0.420	88.260	18.360	36.710	-
Bomag	BPR 50/55 D	0.550	98.090	19.350	38.700	-
Bomag	BPR 70/70 D	0.700	108.140	20.320	40.630	-
Bomag	BPR 100/80 D	0.800	133.810	22.600	45.200	-
MBW	GP1200	0.300	24.100	10.840	21.690	[26]

Table 1. Cont (b) Data for roller compactors.

Manufacturer	Model	Plate width (m)	Total force (kN/m)	$0.45\sqrt{Q\gamma}$	$0.90\sqrt{Q\gamma}$	Referred to
Bomag	BW 55 E	0.559	18.360	8.370	16.740	[10]
Bomag	BW 65 S	0.650	25.600	9.880	19.770	-
Bomag	BW 60 S	0.599	28.570	10.440	20.890	-
Bomag	BW 60 HG	0.599	32.480	11.140	22.270	-
Bomag	BW 60 HD	0.599	32.980	11.220	22.440	-
Wacker	RS 800A	0.719	21.720	9.100	18.210	-
Bomag	BW 75 E	0.749	28.670	10.460	20.920	-
Bomag	BW 35 W	0.391	57.580	14.830	29.650	-
Ingersoll-Rand	DX-60	0.584	38.940	12.190	24.380	-
Bomag	BW 35 W	0.391	58.180	14.900	29.810	-
Bomag	BW 75 AD	0.759	34.850	11.530	23.070	-
Ingersoll-Rand	DX-70	0.635	42.140	12.680	25.370	-
Bomag	75 S	0.749	38.450	12.120	24.230	-
Bomag	90 AD	0.899	35.640	11.660	23.330	-
Wacker	W 55/55T	0.549	67.000	15.990	31.980	-
Wacker	WDH 86-110	0.864	44.160	12.980	25.970	-
Bomag	BW 90 S	0.899	44.970	13.100	26.200	-
Wacker	W 74A	0.749	63.210	15.530	31.070	-
Wacker	W 74/74T	0.749	63.470	15.570	31.130	-
DYNAPAC	CA150PD	1.676	108.710	20.370	40.740	[38]
CATERPILLAR	CW 34	2.090	60.960	15.250	30.510	[13]
CASE	SV212	2.200	158.670	24.610	49.220	[13]
MULLER	VAP55P	1.680	113.100	20.780	41.550	-
MULLER	VAP70P	2.140	149.530	23.890	47.780	-
DYNAPAC	CA134PD	1.370	78.980	17.360	34.730	-
DYNAPAC	CA150PD	1.680	107.990	20.300	40.610	-
DYNAPAC	CA250PD	2.130	173.050	25.700	51.400	-

Note: (a) Total force = compactor weight + dynamic force; compacted soil unit weight average, $\gamma = 19.0 \text{ kN/m}^3$ and (b) Data of compactor was selected based on a previous study conducted by previous authors and Dynapac & Bomag manufactures.

From Table 1a, b the limits of CIS value for unreinforced fill for vibratory plate compactor (light compaction) and roller compactor (heavy compaction) are 14 kPa - 28 kPa and 14 kPa - 30 kPa and for geosynthetic reinforced soil, the CIS values are likely to be higher. Furthermore, Table 1a, b only showed that the width of the plate or roll (w) is from 0.2 m to 0.8 m and from 0.4 m to 2.2 m for vibratory plate compactors and roller compactors, respectively.

In this study, using Bolton's upper limit of CIS values are 28 kPa and 30 kPa or total force/ with, Q (kN/m) are 50 kN/m and 59 kN/m for light compaction and heavy compaction, respectively, for preliminary design in choosing load compaction in numerical modeling of CIS.

3. Compaction-Induce stress

An FE model of a back-to-back GRS wall was developed and verified using a large-scale soil geosynthetic composite (SGC) test that has already been utilised for validation in several other numerical model studies [26-28,35-38]. In this study, SGC Test 2 was selected. The wall was 2 m high, 1.4 m wide ($L/H = 0.7$) and had reinforcement spacing $S_v = 0.2$ m (Figure 2). The backfill was diabase -crushed gravel with a maximum particle size of 33 mm, classified as well-graded gravel (GW) according to the Unified Soil Classification System. Large size triaxial test (specimen diameter = 150 mm; height = 300 mm) results indicated that the backfill had a peak friction angle $\phi = 50^\circ$ and cohesion $c = 70$ kPa for confining pressures between 0 and 200 kPa. The reinforcement was a polypropylene (PP) woven geotextile with an ultimate tensile strength $T_{ult} = 140$ kN/m and axial stiffness $EA = 1000$ kN/m obtained from a wide width tensile test (ASTM D4595). The backfill was placed and compacted to 98% o maximum dry density in 0.2 m.

The FE program PLAXIS 2D v 8.2 [29,31] was selected for the numerical analysis. The zero thickness interface elements were used to simulate the facing/block – backfill – geosynthetic interaction. The values of interface property between soil – reinforcement ($R_i = 0.8$) is valuable in this research. This factor is applied to the adjacent soil's properties as follows:

$$c_i = R_i c_{soil} \quad (4)$$

$$\phi_i = \tan^{-1}(R_i \tan \phi_{soil}) \quad (5)$$

$$\psi_i = \begin{cases} 0 & R_i < 1.0 \\ \psi_{soil} & R_i = 1.0 \end{cases} \quad (6)$$

$$G_i = R_i^2 G_{soil} \quad (7)$$

$$E_{oed,i} = 2G_i \frac{1-\nu_i}{1-2\nu_i} \quad (8)$$

where c_{soil} is the soil cohesion; ϕ_{soil} is the soil friction angle; ψ_{soil} is the soil dilatancy angle, and G_{soil} is the soil shear modulus.

Table 2 shows the input parameters used in this study. The wall was constructed in stages, i.e., 0.15m thick soil lifts were placed and compacted until the final wall height was reached. A fixed boundary condition in the horizontal direction was applied to the right lateral border. At the bottom of the model, a fixed boundary condition was employed in both the horizontal and vertical directions.

The FE analysis was conducted by following two construction stages (i.e., staged construction and compaction and applied service load at the surface of the SGC mass). Compaction of each soil lift was simulated by applying an equivalent compaction pressure of applying a distribution load at the top of each backfill layer or application a distribution load at the top and bottom of each soil layer and removed the applied compaction pressure before placing the next soil lift. The maximum value of the compaction pressure that related to using Bolton's upper limit theory is 50 kN/m used in the FE model (for the case light compaction)

Figures 2 illustrate the geometry configuration, loading conditions and interface element of an SGC mass, for FE model in a 2m high GRS mass (for light compaction). In FE model, fixed boundary conditions in both the horizontal and vertical directions were employed at the wall bottom. The applied

fixed boundary conditions can be justified by nearly no lateral displacement observed at the wall bottom because of the high friction resistance of the concrete floor slab.

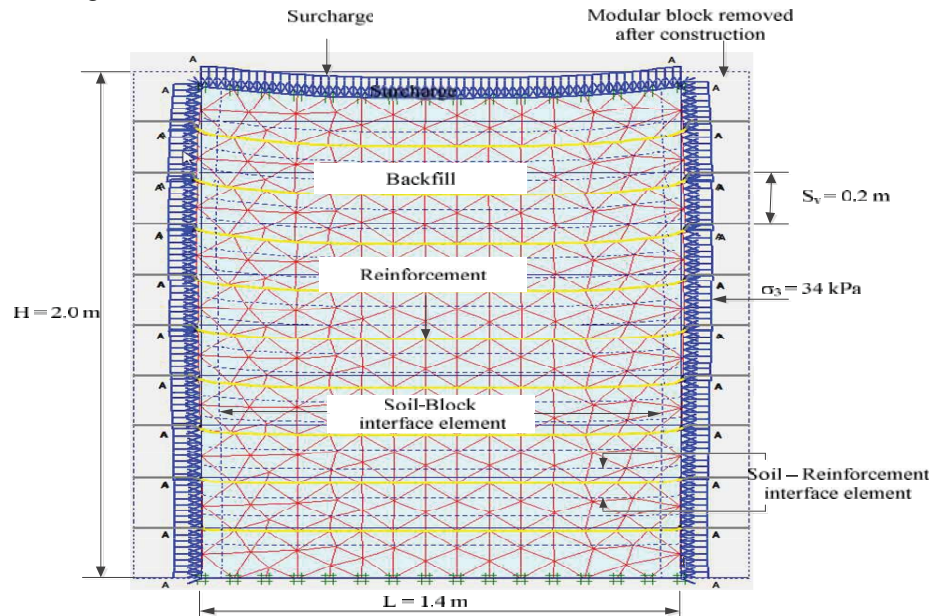


Figure 2. FE mesh and dimensions in Plaxis 2D.

Table 2. The input parameters of FEM modeling.

Material	Value
^(a)Soil properties	
Model	Hardening Soil
Peak plane strain friction angle, ϕ ($^{\circ}$)	50
Cohesion, c (kN/m^2)	70
Dilation angle, Ψ ($^{\circ}$) ^a	19
Unit weight, γ (kN/m^3)	25
$E_{\text{ref}}^{50 \text{ a}}$ (kN/m^3)	62374
$E_{\text{ur}}^{50} = 3 * E_{\text{ref}}^{50}$ (kN/m^3)	187122
Stress dependence exponent, m	0.5
Failure ratio, R	0.8
Poisson's ratio, ν	0.2
P_{ref} (kN/m^2)	100
Reinforcement	
Elastic axial stiffness (kN/m)	1000
Reinforcement spacing (m)	0.2

Table 2. Cont.

^(b)Modular block properties	
Model	Model Linear elastic
Stiffness modulus ((kN/m ²))	3*10 ⁶
Unit weight, γ (kN/m ³)	12.5
Poisson's ratio, ν	0
^(c)Block-Block interface	
Model	Mohr-Coulomb
Stiffness modulus ((kN/m ²))	3*10 ⁶
Unit weight, γ (kN/m ³)	0
Poisson's ratio, ν	0.45
Angle of internal friction, ϕ (°)	33
Cohesion, c (kN/m ²)	2
^(c)Soil -Block interface	
Model	Mohr-Coulomb
Unit weight, γ (kN/m ³)	0
Poisson's ratio, ν	0.45
The angle of internal friction, ϕ (°)	33.33
Cohesion, c (kN/m ²)	46.67
Stiffness modulus (kN/m ²)	74829.711
^(c)Soil -Soil interface	
Model	Mohr-Coulomb
Unit weight, γ (kN/m ³)	0
Poisson's ratio, ν	0.45
Angle of internal friction, ϕ (°)	40
Cohesion, c (kN/m ²)	56
Stiffness modulus (kN/m ²)	106685.26
Geometric configuration	
H, wall height (m)	2
L/H, wall aspect ratio	0.7
Sv, reinforcement vertical spacing (m)	0.2

^(a) The data of soil in Model was selected based on triaxial testing by [26].

^(b) The data of the facing block was selected based on a previous study conducted by [26].

^(c) Defined interface elements with zero thickness in [29].

4. Numerical compaction modelling

Different methods were employed for modeling the compaction induced stress as follows:

- Type I - Applying a uniform distributed load to the top of each backfill soil layer as the wall was being modeled from the bottom up (referred to as procedure type I, see Figure 3a).
- Type II - Applying a uniformly distributed load at the top and bottom of each soil layer, as suggested by [22] (referred to as procedure type II, see Figure 3b).
- Type III - Modeling was also performed using different widths of strip load applied to the top of each backfill layer as the wall was being built from the bottom up. Three different widths of strip loads, w , are considered in this study: 0.7, 0.35, and 0.175m. Besides, the stress paths of typical fill compaction operation are discussed, including compaction with a plant moving away and toward from a section under consideration (hereafter referred to as procedure Type IIIa and type

IIIb see Figure 3c, Figure 3d. Note that in Type of IIIa, or IIIb was for the direction of the movement of a compactor (a) Moving toward Section and (b) Moving away from.

For the numerical modeling of compaction, the range of uniformly distributed load to model the CIS in FE model was from 10 kPa to the maximum value load of 70 kPa.

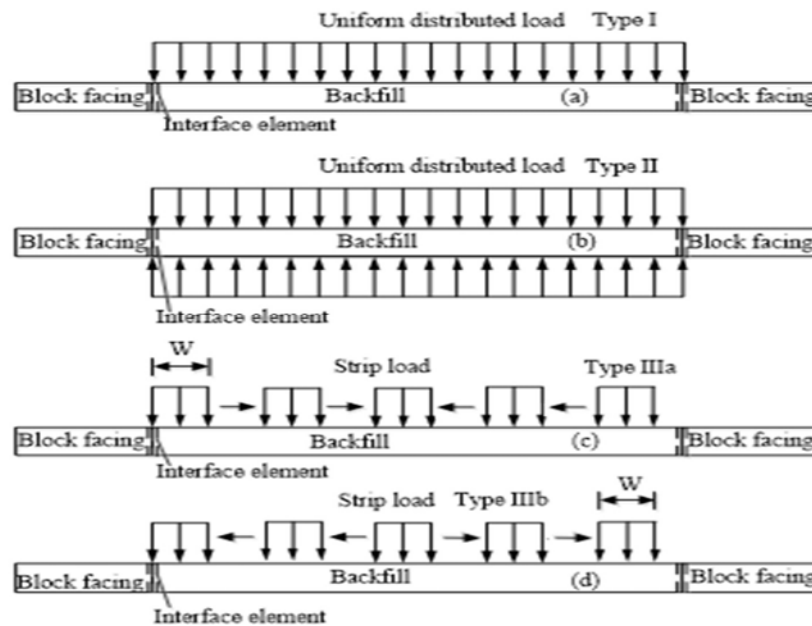


Figure 3. Compaction procedures employed in the numerical analyses for SGC mass for light compaction in FE model ($H = 2.0$ m, $L = 1.4$ m).

5. Results and discussion

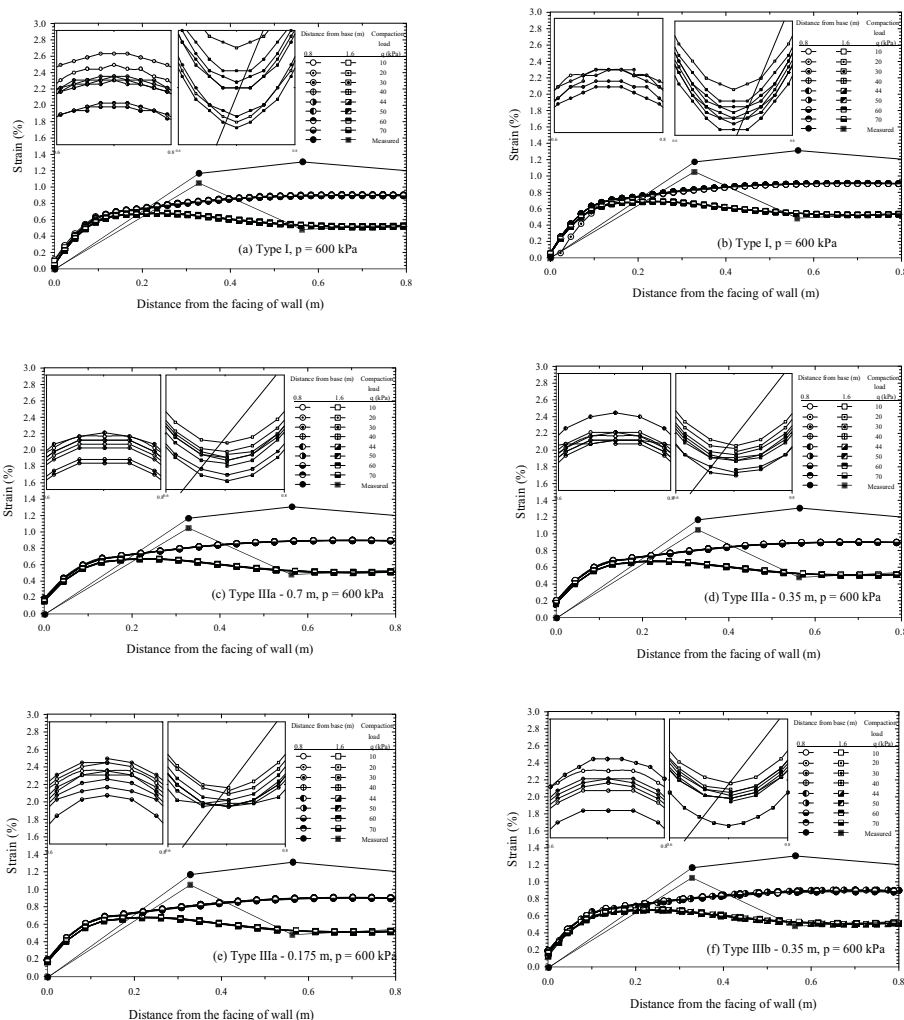
5.1. The axial strain of reinforcement

Figure 4 (a-g) shows the reinforcement strains at the reinforcement layer 0.8 m and 1.6 m from the base, under the applied service load, in which case $p = 600$ kPa at the surface of the specimen by applying the different compaction pressures of each soil lift. The results of the numerical analyses were also compared with the measurements presented by Pham (2009). The results correspond to numerical analyses of the different procedures used for modeling CIS; i.e. type I, type II, type IIIa-0.7m, type IIIa-0.35m, type IIIa-0.175m, type IIIb-0.7m, type IIIb-0.35m, and type IIIb-0.175m. Note that in Type IIIb-0.7 and Typ b-0.7m we have the same value because we have a mirror of FE modeling see Figure 2.

Figure 4 (a-g) also shows that the simulated strains for seven cases of compaction simulation procedures are in good agreement with the measured data for reinforcement layers located at 1.6 m and 0.8 m from the base with case $p = 600$ kPa for all compaction pressure values ($q = 10, 20, 30, 40, 44, 50, 60$ and 70 kPa) when compaction procedures of all the type was employed under staged construction and compaction and applied service load. Note that the compaction pressure of 44 kPa was obtained from the actual plate compactor used in the SGC tests 2 (Whacker VPG-155A) and 70 kPa was an optimized load for plate compactor that is chosen from FEM trial method until SGC failure occurred. Furthermore, the compaction load has different influences depending on the magnitude of compaction loads. The value of lateral displacement fell slowly when applying the compaction load from 10 to 40 kPa but later decreased substantially and hit the lowest point ($q = 70$ kPa) when decreasing the compaction load from 40 to 70 kPa. For Type I, $p = 600$ kPa, $q = 10$ kPa (Figure 4a) the axial strain was 0.911 mm at the layer 0.8m and 0.684 mm at layer 1.6m. Increasing the compaction load to 40 kPa, the axial strain of reinforcement at the layers 0.8m and layer 1.6 m decreased to 0.908 mm and 0.685 mm,

respectively. When the compaction load was 70 kPa, the axial strain of reinforcement at the layer 0.8m and layer 1.6 m dropped significantly to 0.900 and 0.679 mm, respectively. The axial strain from another kind of compaction procedure i.e. Type II and Type III (IIIa-0.7m, IIIa-0.35m, IIIa-0.175m, IIIb-0.35m, IIIb-0.175m) follow the same pattern (See Figure 4(b-g)). This result only shows that the effective compaction load of compactor for plate compactor was $q > 40$ kPa. And this result may also imply that the difference in the compaction load might be insignificant to one of the characteristics of the stress-deformation behavior of this SGC mass is the axial strain. These studies indicated that with $q > 40$ kPa, the CIS will result in a significant increase in the increasing lateral stress of a soil mass. The increase in lateral stresses due to compaction during construction will lead to an increase in the stiffness and strength of the soil mass that leads to less than the axial strain in each other reinforcement layer.

In comparison, there is a significant difference in this study compared to the case study by [23]. When the compaction was simulated by applying a distribution load at the top and bottom of each soil layer (compaction procedure Type II) satisfactory agreement has been generally observed between measurements and calculated values. Therefore, procedure Type II is suggested for the modeling of CIS, but in this case, the effect of compaction procedure Type II is not significant to the composite behavior of SGC mass when compared with another compaction procedure (Referred to Type I and Type III).



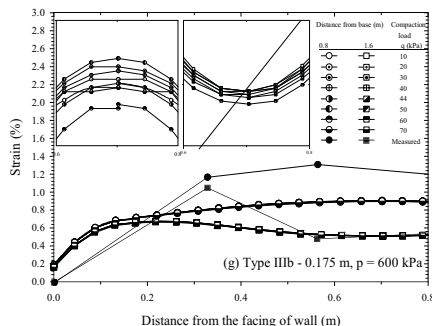
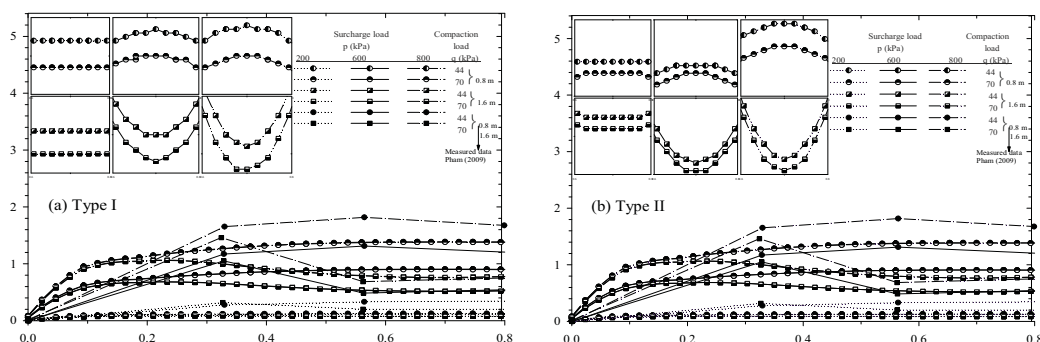


Figure 4 (a-g). Reinforcement strains of SGC Test 2 mass at reinforcement layer 0.8 m and 1.6 m from the base, case $p = 600$ kPa with different compaction load $q = 10 \sim 70$ kPa.

Figure 5 (a-g) shows the axial strain of reinforcement under three different pressures at the surface of the specimen with applying the different compaction pressures of each soil lift ($q = 44$ and 70 kPa) under the applying the uniformly different distributed surcharge loads were applied to the top surface of the specimen at three different magnitudes ($p = 200, 600$ and 800 kPa). The numerical results are in good agreement with the measured data and show the composite behavior of GSC mass for all surcharges load applied to the top surface of the specimen by [26]. For Type I, $p = 200$ kPa (Figure 5a), the reinforcement strain from $p = 200$ was 0.089% at the layer 1.6 m and increased to 0.124% at layer 0.8 m. Increasing the compaction load $q = 70$ kPa, the axial strain of reinforcement at the layer 0.8 m and layer 1.6 m fell considerably to 0.087% and 0.123% , respectively. There were the same results with case surcharge loads $p = 600$ and 800 kPa. And the results also showed that an increase in the surcharge load from $p = 200$ kPa to $p = 800$ kPa will increase the reinforcement strain at both positions of the reinforcement of 0.8 m and 1.6 m, respectively.

Similarly, we had the same results for another compaction procedures of Type II and Type III (See Figure 5 (b-g)). Furthermore, there are small value differences between the compaction procedures. For example, for $p = 200$ kPa the maximum variation between the numerical results of the seven compaction procedures are 6.23% and 6.50% at the layers of 0.8 m and 1.6 m, respectively and similarly for $p = 800$ kPa, $q = 44$ kPa the maximum variation between the numerical results of the seven compaction procedures are 2.35% and 2.89% at the layers of 0.8 m and 1.6 m, respectively. The results thus suggested that the consideration of different compaction simulation procedures on the reinforcements strains in SGC mass could be neglected in the future numerical simulation.



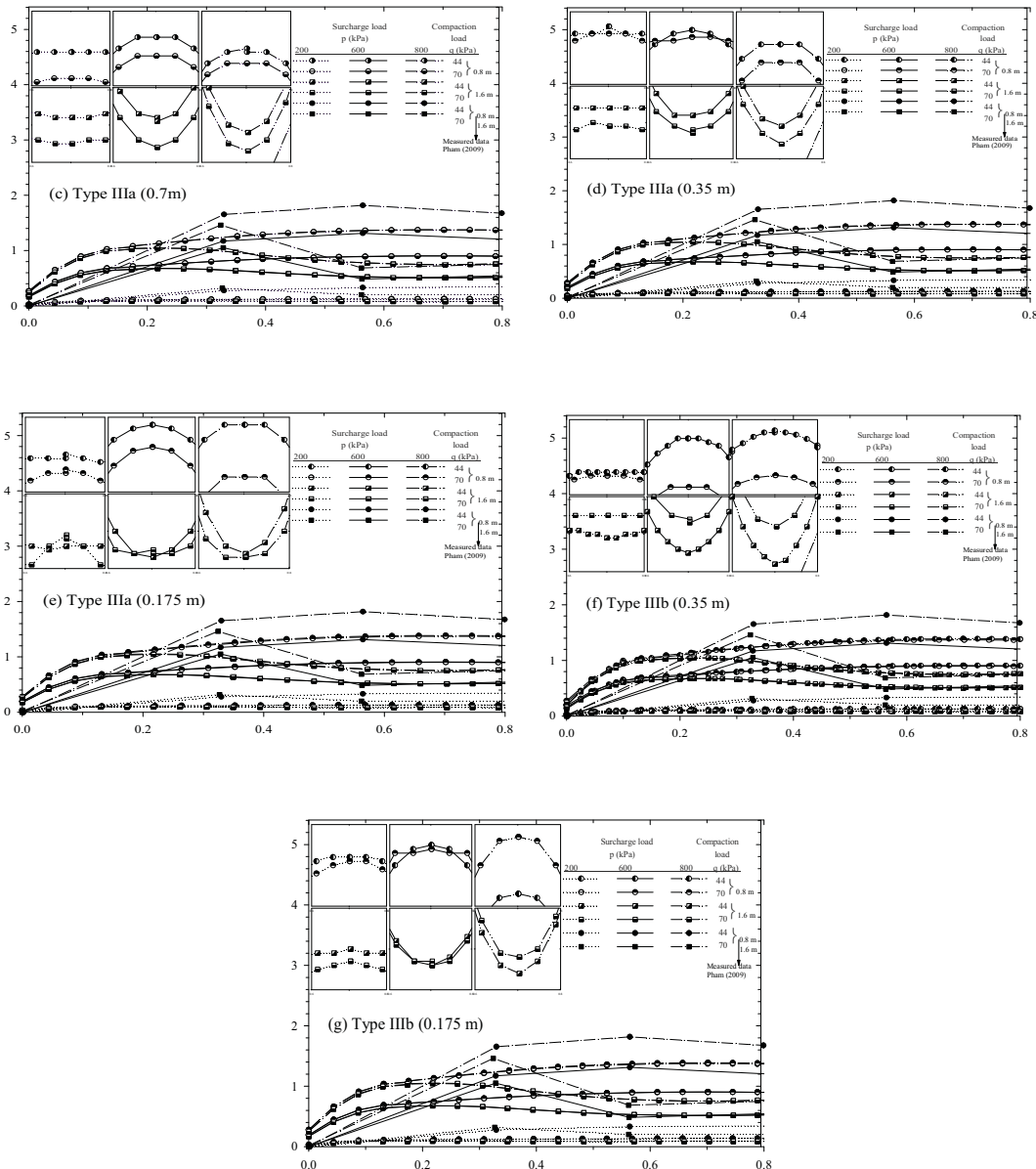


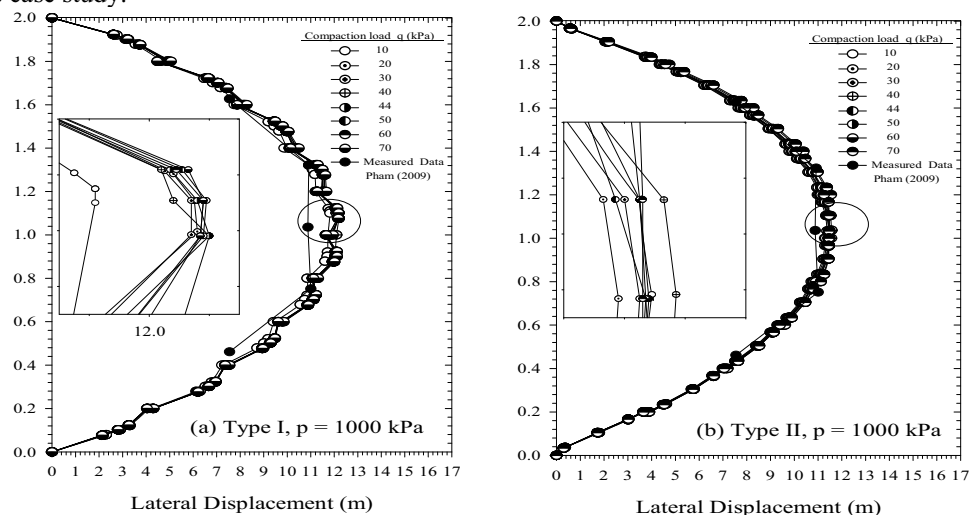
Figure 5 (a-g). Comparison of reinforcement strains of SGC Test 2: At reinforcement layer 0.8 m and 1.6 m from the base, case $p = 200, 600,$ and 800 kPa with compaction load $q \geq 40$ kPa ($p = 44$ and 70 kPa).

5.2. Lateral displacements on the open faces of the specimen

Figure 6 (a-g) shows the lateral displacements on the open faces of the specimen at $x = 0.2$ m from the facing with the uniformly distributed surcharge load was applied to the top surface of the specimen at magnitude $q = 1000$ kPa by applying the different compaction pressures of each soil lift $q = 10, 20, 30, 44, 50, 60$ and 70 kPa. In Figure 6 (a-g), the results also correspond to numerical analyses of the different procedures used for modeling CIS, i.e., type I, type II, type IIIa-0.7m, type IIIa-0.35m, type IIIa-0.175m, type IIIb-0.35m, and type IIIb-0.175m.

Figure 6 (a-g) indicates that the numerical results are in good agreement with the measured data with case $p = 1000$ kPa for all compaction pressure values ($q = 10, 20, 30, 40, 44, 50, 60$ and 70 kPa). Note that the compaction pressure of 44 kPa was obtained from the actual plate compactor used in the SGC tests and 70 kPa was the maximum compaction pressure for plate compactor. The compaction load has different influences depending on the magnitude of compaction pressures. The value of lateral displacement fell slowly when applying the compaction pressure q from 10 to 40 kPa but later decreased substantially and hit the lowest point ($q = 70$ kPa) when decreasing the compaction pressure from 40 to 70 kPa. For example, in Type II, $p = 1000$ kPa, $q = 10$ kPa, (Figure 6b) the lateral displacement was 11.49 mm. Increasing the compaction load to 40 kPa, the lateral displacement decreased to 11.48 mm. When the compaction load was 70 kPa, the lateral displacement of facing fell slowly to 11.47 mm, respectively.

The lateral displacement measured by FE method from another compaction process (ie., Type II and Type III (IIIa- 0.7 m, IIIa- 0.35 m, IIIa- 0.175 m, IIIb- 0.35 m, IIIb- 0.175 m)) give the same results (See Figure 5(a-g)). This result only shows that the effective compaction pressure of the plate compactor was $q \geq 40$ kPa. And this result may also imply that the difference in the compaction load might be insignificant to one of the characteristics of the stress-deformation behavior of this SGC mass is the lateral displacement. These studies indicated that with $q \geq 40$ kPa, the CIS will result in a significant increase in the increasing lateral stress of a soil mass. The increase in lateral stresses due to compaction during construction will lead to an increase in the stiffness and strength of the soil mass that leads to less than the lateral displacement. The effect of the magnitude of compaction pressure of each soil lift, case $q < 40$ kPa is not significant to characteristics of composite behavior (referred lateral displacement). These results can be explained by the compaction energy in this case study that related to soil type, depth of the soil layer, moisture, and density of the backfill soil, is not sufficient. in this case study.



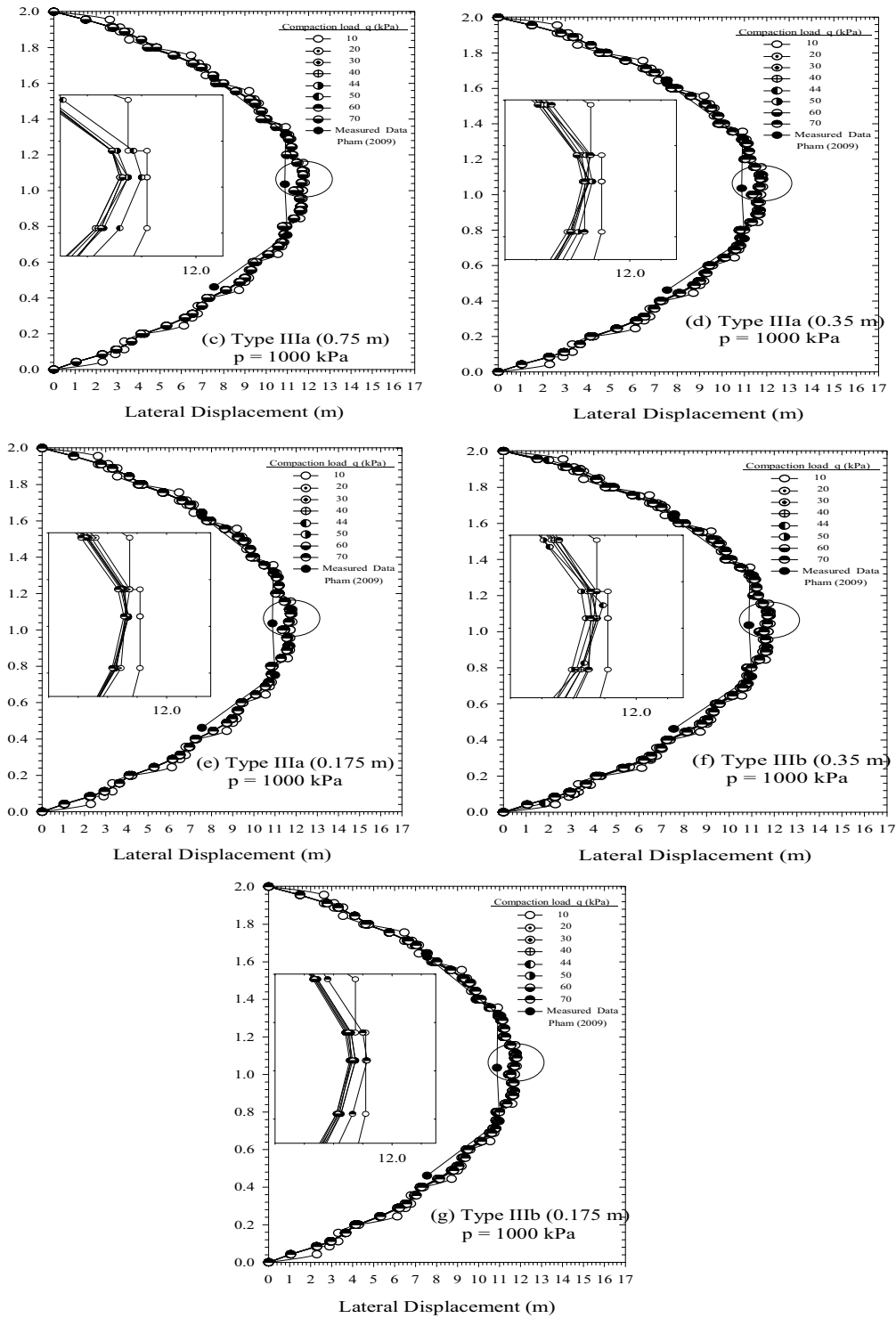
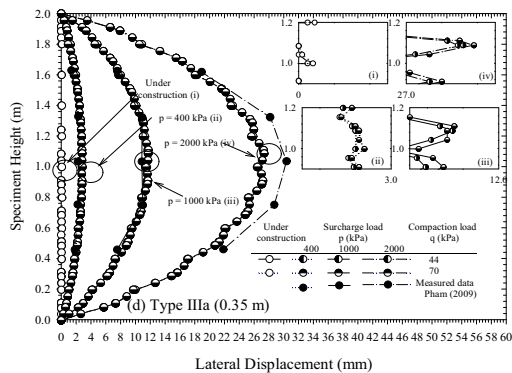
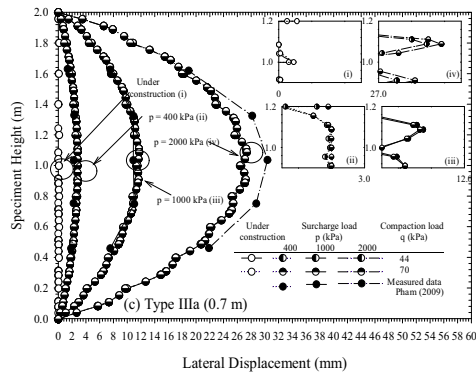
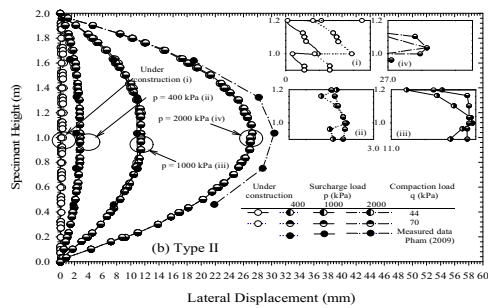
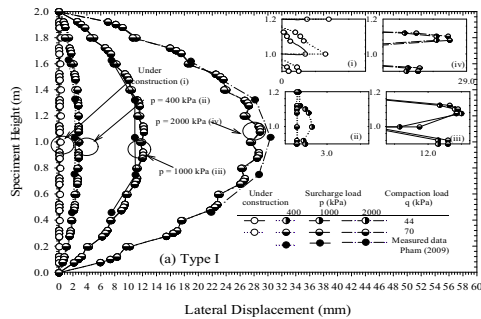


Figure 6 (a-g). Lateral Displacement at Open Face of SGC Test 2, case $p = 1000$ kPa.

Figure 7 (a-g) show that the lateral displacements on the open faces of the specimen at the four

different pressures at the surface of the specimen by applying the different compaction pressure of each soil lift ($q = 44$ and 70 kPa) under the applying the uniformly different distributed surcharge load was applied to the top surface of the specimen at four different magnitudes ($p = 400, 1000,$ and 2000 kPa). It is noted that in this analysis, The FE analysis was conducted by following two construction stages (i.e., staged construction and compaction, and applied a service load at the surface of the SGC mass). Overall, the numerical results are in good agreement with the measured data and show the composite behavior of GSC mass for all surcharge load applied to the top surface of the specimen. For example, in service load stage (Figure 7(a-g)), for Type I, the horizontal displacement jumped from 2.83 mm ($p = 400$ kPa) to 12.20 mm ($p = 1000$ kPa), and 28.82 mm ($p = 2000$ kPa) with the compaction load $q = 44$ kPa. Increasing the compaction load $q = 70$ kPa, the horizontal displacement fell considerably from 2.82 mm ($p = 400$ kPa) to 12.18 mm ($p = 1000$ kPa) and 28.77 mm ($p = 2000$ kPa). In contract, in staged construction and compaction, for type I, the horizontal displacement increased from 0.22 mm to 0.33 mm. Similarly, we had the same results for another compaction procedure type II, III (Figure 7(b-f)). The difference of tending of lateral displacement in two-stage showed the behavior of SGC mass that the vertical compaction pressure can cause an increasing lateral displacement on the open faces of the specimen in staged construction and compaction stages but it will bring about an increase in the lateral stress, provided that there is sufficient constraint to lateral deformation of the soil mass, is referred to as “compaction-induced stress” (CIS). Additionally, the small value of lateral displacement on the faces of the specimen in staged construction and compaction stages can be explained that the lateral displacement of SGC mass was constrained by the rigid concrete facing blocks in the wall model. Moreover, the maximum variation between the numerical results of the seven compaction procedures are 4.6% for $p = 400$, 5% for $p = 1000$ kPa, and 5% for $p = 2000$ kPa. The results thus suggested that the consideration of different compaction simulation procedures on the lateral displacement in SGC mass could be neglected in future numerical simulations.



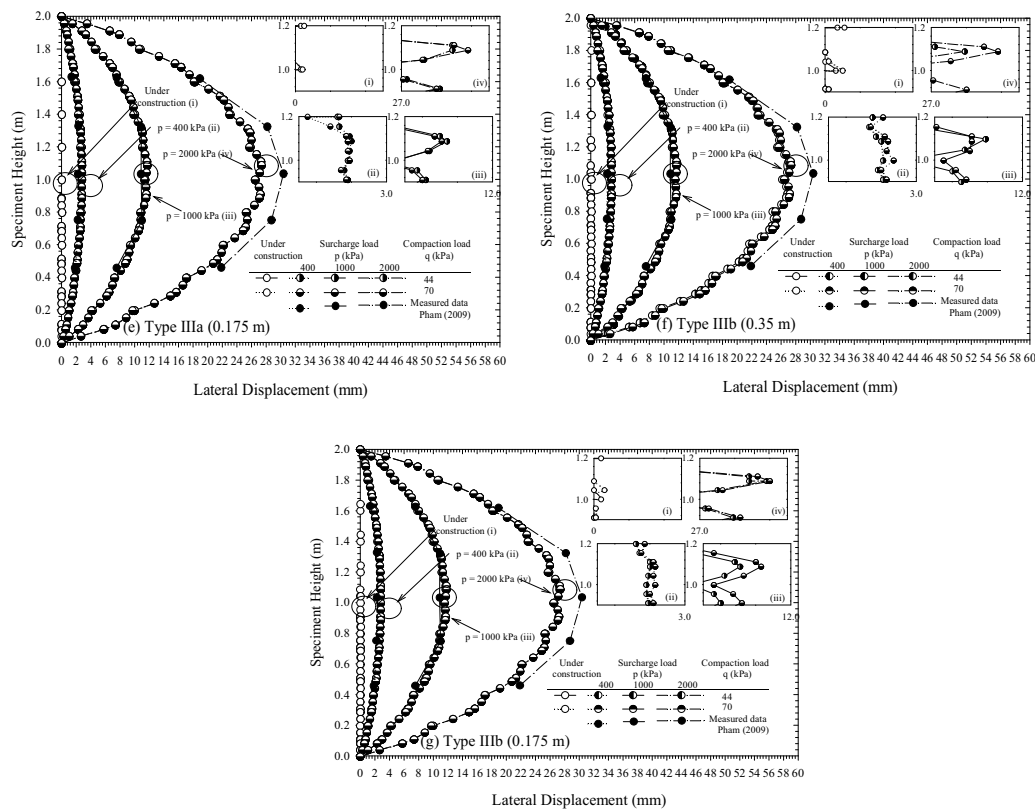


Figure 7 (a-g). Comparison of lateral displacement of SGC Test 2 for two stage constructions: Under construction and surcharge load in both compaction load ($q = 44$ kPa, $q = 70$ kPa).

6. Conclusions

This paper presents two numerical modelings of a soil geosynthetic composite (SGC) mass that was carried out from a large-scale soil geosynthetic composite (SGC) test by [26]. Although it has been used for validation in several other numerical model studies, all of those studies used the real value of the compaction specified for the vibrating plate compactor (44 kPa). In this study, Bolton's upper limit of the CIS value for both light compaction and heavy compaction was used for preliminary design in choosing load compaction in numerical modeling of CIS. The results of the numerical analyses using different compaction modeling procedures were compared with the measured values of the lateral displacements, reinforcement strains during all stages of SGC mass construction. Based on the cases and conditions examined, the following conclusions are made:

- Using Bolton's upper limit of CIS values of 28 kPa and 30 kPa, or total force, Q (kN/m) is 50 kN/m and 59 kN/m for light compaction and heavy compaction in choosing the maximum load compaction for each backfill layer in numerical modeling of CIS may be adopted for the preliminary design and analysis of SGC structures.
- For FE model in case of light compaction, with the effective compaction load of compactor $q \geq 40$ kPa, the predicted reinforcement strains and lateral displacements generally agreed well with measurement data (Pham, 2009). There is an insignificant effect of using different compaction modeling procedures (i.e., Type I, Type II, IIIa-0.7m, IIIa-0.35m, IIIa-0.175m, IIIb-0.35m, and IIIb-0.175m) and the magnitude of compaction pressure due to very small differences in predicted reinforcement strains and lateral displacements. (Shown in Figure 4 (a-g), Figure 5(a-g), Figure 6(a-g), Figure 7(a-g)). These results suggested that the consideration of different

compaction procedures for the distribution of strains in the reinforcement and lateral displacement in SGC mass may be neglected in this analysis.

- The numerical analysis in which the compaction was simulated using a strip load applied to the top of each backfill layer (compaction procedure type III) indicates that the reinforcement strains and lateral displacements using compaction procedure type III, depending on the width of the strip load, using the 0.7-meter-side strip load (Type III-0.7m) gave the highest value when compared with other cases (i.e., Type III-0.35m and Type III-0.175m). Furthermore, the different movements of the load (between Type IIIa and Type IIIb) might be insignificant to reinforcement strains and lateral displacements.

References

- [1] Adams, M T et al 2002 Vegas Mini Pier Experiment and Postulate of Zero Volume Change *Seventh International Conference on Geosynthetics* (Nice) 389–394
- [2] Adams, M T, Schlatter, W and Stabile, T 2007 Geosynthetic-Reinforced Soil Integrated Abutments at the Bowman Road Bridge in Defiance County *Ohio Proceedings* (Geo-Denver: ASCE)
- [3] Aggour, M S and Brown, C B 1974 The Prediction of Earth Pressure on Retaining Walls Due to Compaction, *Geotechnique* **24** 489–502
- [4] American Association of State Highway and Transportation Officials AASHTO 2014 *LRFD Bridge Design Specifications 7th edn*
- [5] Bathurst, R J A et al 2009 Influence of reinforcement stiffness and compaction on the performance of four geosynthetic-reinforced soil walls *Geosynthetics International* **16** 43–59
- [6] Berg, R R, Christopher, B R and Samtani, N 2009 Design of Mechanically Stabilized Earth Walls and Reinforced Soil Slopes *Design & Construction Guidelines Report No FHWA-NHI-00-043 McLean*
- [7] Bolton, M 1991 Geotechnical Stress Analysis for Bridge Abutment Design *Transportation Research Laboratory Contractor Report* (London)
- [8] Bomag 2020
- [9] Broms, B 1971 Lateral pressure due to compaction of cohesionless soils *Proc 4th Budapest Conf SMFE* 373–384
- [10] Duncan, B J M et al 1991 Estimation earth pressures due to compaction *Journal of Geotechnical Engineering* **117** 1833–1847
- [11] Duncan, J and Seed, R 1986 COMPACTION-INDUCED EARTH PRESSURES UNDER Ko-CONDITIONS *Journal of Geotechnical Engineering* **112** 1–22
- [12] Dynapac 2020
- [13] Ehrlich, M and Becker, L 2010 Reinforced Soil Walls and Slopes: Design and Construction Abingdon (UK: Taylor & Francis)
- [14] Ehrlich, M and Mitchell, J K 1994 WORKING STRESS DESIGN METHOD FOR REINFORCED SOIL *Journal of Geotechnical Engineering* **120**
- [15] Elton, D J and Patawaran, M A B 2005 Mechanically Stabilized Earth MSE Reinforcement Tensile Strength from Tests of Geotextile Reinforced Soil *Technical Report*
- [16] Hatami, K and Bathurst, R J 2005 Development and verification of a numerical model for the analysis of geosynthetic-reinforced soil segmental walls under working stress conditions *Canadian Geotechnical Journal* **42** 1066–1085
- [17] Hatami, K and Bathurst, R J 2006 Numerical model for reinforced soil segmental walls under surcharge loading *Journal of Geotechnical and Geoenvironmental Engineering* **132** 673–684
- [18] Holtz, R D and Lee, W F 2002 Internal Stability Analyses of Geosynthetic Reinforced Retaining Walls, *Washington State Transportation Center TRAC*
- [19] Ketchart, K and Wu, J T H 2001 Performance Test for Geosynthetic-Reinforced Soil Including Effects of Preloading *Federal Highway Administration*
- [20] Mirmoradi, S H and Ehrlich, M 2014 Modeling of the compaction-induced stresses in numerical analyses of grs walls *International Journal of Computational Methods* **112** 1–14

- [21] Mirmoradi, S H and Ehrlich, M 2015a Compaction-induced stress: numerical modeling, *15th Pan-American Conference on Soil Mechanics and Geotechnical Engineering* (Buenos Aires, Argentina)
- [22] Mirmoradi, S H and Ehrlich, M 2015b Modeling of the compaction-induced stress on reinforced soil walls *Geotextiles and Geomembranes* **43** 82–88
- [23] Mirmoradi, S H and Ehrlich, M 2018 Numerical simulation of compaction-induced stress for the analysis of RS walls under working conditions *Geotextiles and Geomembranes* **46** 354–365
- [24] National Concrete Masonry Association NCMA 2009 *Design Manual for Segmental Retaining Walls 3rd edn*
- [25] Nicks, J E, Adams, M T and Ooi, P S K 2013 Geosynthetic reinforced soil 1 performance testing – Axial load deformation relationships *Report No FHWA-HRT-13-066* McLean
- [26] Pham, T 2009 Investigating Composite Behavior of Geosynthetic-Reinforced Soil Grs Mass *University of Colorado at Denver*
- [27] Gui, MW, Phan, TTT and Pham, QT 2020 Impacts of Compaction Load and Procedure on Stress-Deformation Behaviors of a Soil Geosynthetic Composite SGC Mass—A Case Study *Applied Sciences* **10** 6339
- [28] Phan, T T T, Gui, M W and Pham, Q T 2021 Numerical Simulation of Compaction Load on Stress Deformation Behavior of Soil Geosynthetic Composite Mass *Advances in Transportation Geotechnics IV LNCE 165* In *Advances in Transportation Geotechnics IV: Proceedings of the 4th International Conference on Transportation Geotechnics*; Tutumluer, E, Nazarian, S, Al-Qadi, I, Qamhia, IIA, Eds; Springer: Berlin/Heidelberg, Germany **2** 945–956
- [29] Plaxis 2D 2002 *Plaxis 2D - Version 8 Manual* Rotterdam: Balkema
- [30] Rowe, R K and Ho, S K 1998 Horizontal deformation in reinforced soil walls *Canadian Geotechnical Journal* **35** 312–327
- [31] Schanz, T, Vermeer, P and Bonnier, P 1999 The Hardening Soil Model: Formulation and Verification *Beyond 2000 in computational geotechnics* 281–296
- [32] Seed, R 1983 Compaction-induced Stresses and Deflections on Earth Structure *University of California at Berkeley*
- [33] Seed, R and Duncan, J 1986 FE ANALYSES: COMPACTION-INDUCED STRESSES AND DEFORMATIONS *Journal of Geotechnical Engineering* **112** 23–43
- [34] Wu, J T H 2001 Revising the AASHTO Guidelines for Design and Construction of GRS Walls *Report No CDOT-DTD-R-2001-6*
- [35] Wu, J T H et al 2011 Required minimum reinforcement stiffness and strength in geosynthetic-reinforced soil GRS walls and abutments, *International Journal of Geotechnical Engineering* **54** 395–404
- [36] Wu, J T H et al 2014 Suppression of Soil Dilatation—A Reinforcing Mechanism of Soil-Geosynthetic Composites, *Transportation Infrastructure Geotechnology* **11** 68–82
- [37] Wu, J T H et al 2018 Analysis of Stress-Deformation Behavior of Soil-Geosynthetic Composites in Plane Strain Condition *Transportation Infrastructure Geotechnology* **5**
- [38] Wu, J T H, Hoffman, P and Pham, T Q 2018 “Numerical simulation of compaction-induced stress for the analysis of GRS walls under working conditions” by S H Mirmoradi and M Ehrlich *Geotextiles and Geomembranes* **46** 354–365
- [39] Wu, J T H and Pham, T Q 2010 An analytical model for evaluation of compaction-induced stresses in a reinforced soil mass *International Journal of Geotechnical Engineering* **4** 549–556
- [40] Wu, J T H and Pham, T Q 2013 Load-carrying capacity and required reinforcement strength of closely spaced soil-geosynthetic composites *Journal of Geotechnical and Geoenvironmental Engineering* **139** 1468–1476
- [41] Yang, K H et al 2016 Lateral bearing capacity and failure mode of geosynthetic-reinforced soil barriers subject to lateral loadings *Geotextiles and Geomembranes* **44** 799–812
- [42] Yu, Y, Bathurst, R and Allen, T 2016 Numerical modeling of the SR-18 geogrid reinforced modular block retaining walls *Journal of Geotechnical and Geoenvironmental Engineering* **142** 1–13

- [43] Yu, Y, Bathurst, R and Allen, T 2017 Numerical modelling of two full-scale reinforced soil wrapped-face walls *Geotextiles and Geomembranes* **45** 237–249
- [44] Thang Pham, S Mustapha Rahmaninezhad, Andres Palma, Truc Phan, and Thuy Vu 2023 Analytical Method for Predicting Lateral Facing Deflection of Geosynthetic-Reinforced Soil Abutment Walls *Geo-Congress* 345-358